Mon. Not. R. astr. Soc. (1980) **190**, 551–574

Neutral hydrogen in the Andromeda Nebula – I. H I emission in the south-west region of the nebula

S. C. Unwin *Mullard Radio Astronomy Observatory, Cavendish Laboratory, Madingley Road, Cambridge CB3 0HE*

Received 1979 August 3; in original form 1979 June 27

Summary. Aperture synthesis observations of the south-west region of the Andromeda Nebula (M31) have been made in the neutral hydrogen line using the Cambridge Half-Mile Telescope, with a synthesized beam of 0.8 × 1.2 arcmin, and a resolution in radial velocity of 16 km s^{-1}. Most of the H I gas exists in narrow arm-like features which are well separated except near the minor axis, and which can be detected up to ~ 25 kpc from the nucleus. A comparison with the distribution of optical emission shows that H I is highly correlated with dust lanes on scales ~ 100 pc, and also with H II regions and OB associations, in good agreement with earlier work by Emerson. No obvious spiral pattern, whether leading or trailing, can be traced in the distribution of H I gas. H I absorption has been detected in the direction of the continuum source 5C 3.107, and the implied spin temperature is ≈ 220 K. A detection of H I emission in the elliptical companion galaxy NGC 205 is reported.

1 Introduction

High-resolution H I observations of spiral galaxies provide an important test for theories of spiral structure, which must explain the spatial distribution of H I gas, its velocity structure and its relation to other tracers of spiral arms such as OB associations and H II regions. Several surveys of nearby spiral galaxies have been made in recent years (e.g. M31, Emerson 1974, 1976; Shane 1975a; M33, Newton 1978; M51, Shane 1975b; M81, Rots & Shane 1975; M101, Allen & Goss 1979). An essential feature of these investigations is the use of aperture synthesis techniques to provide sufficient angular resolution for the separation of adjacent spiral arms. The local group members M31 and M33 can be studied in the greatest detail, and M31 is particularly important as it is believed to be similar to our Galaxy in many respects.

This paper presents maps of the integrated hydrogen emission within an area of 2.9 deg^2 in the south-west region of M31, and describes the detailed spatial distribution of H I in relation to dust, OB associations, H II regions etc. Although the H I observations of Shane (1975a) were of higher angular resolution than those of the present survey, only a relatively

small region near the nucleus of M31 was mapped, with incomplete sampling of the velocity information. The new H I survey is more sensitive than that of Emerson (1974), and has a smaller synthesized beam size and improved resolution in radial velocity; it reveals complicated small-scale structure on scales ~ 100 pc which has not been seen previously.

Section 2 describes the details of the survey and the methods of data reduction, and Section 3 presents maps of integrated hydrogen emission made with beamwidths of 0.8×1.2 and 1.9×2.9 arcmin. Detailed comparisons of these maps with optical emission, dust, H II regions, OB associations and CO detections are made in Section 4. Section 5 discusses the evidence for a large-scale spiral pattern traced by H I arm segments and other spiral arm tracers, and Section 6 summarizes the main conclusions of the paper. A second paper will present the velocity field of this survey, and the dynamics of neutral hydrogen in the disc of M31 will be discussed.

2 Observations and data reduction

Table 1 gives the observational details of the survey made with the Cambridge Half-Mile telescope. Most of the H I gas in M31 lies in a broad ring of radius ~ 10 kpc, and the map centre of the survey was chosen so that the southern half of this 'ring' lay within the half-power primary beam response of the telescope. The survey was calibrated by observations of 3C 119, whose flux density was taken to be 8.6 Jy (Gillespie 1974), and which is believed to be free of galactic emission and absorption over the range of baselines and frequencies observed.

Since the smallest interferometer spacing used was 12.2 m (58 λ), the aperture plane coverage was not quite complete; the 6.1-m spacing cannot be observed with the 9.1-m paraboloids of the Half-Mile telescope. This has two effects on the 'output maps' obtained by Fourier inversion of the spectrometer data:

(i) angular structure on scales $\gtrsim 1^\circ$ is attenuated, and no structure on scales $\gtrsim 2^\circ$ can be detected;

(ii) variations of zero level are introduced, and the true brightness distribution lies in a bowl-shaped depression.

Correction of (i) requires the use of single-dish observations to reconstruct the missing spatial frequencies, but this has not been attempted because of a lack of suitable low-resolution data. Large-scale features have been studied by several authors (Roberts 1966; Emerson 1974), but these are not the main concern of the present survey. A comparison of these observations with the H I survey by Emerson showed that the integrated H I intensity of any missing structure due to (i) is $\lesssim 100\,\mathrm{K\,km\,s^{-1}}$. Zero-level variations (ii) affect the measurement of integrated hydrogen emission, and were corrected by model-fitting the observed 12.2- and 18.3-m spacings to construct the 6.1-m spacing (Newton 1978). In this way, only large-scale structure for which there is good evidence from the observations is added to the map. Residual spurious structure is much smaller than the receiver noise level of the high-resolution maps.

Output maps were made at three angular resolutions, and the rms noise levels are given in Table 1. None of the maps was confused by grating responses and no rings due to distant strong sources were found. Continuum emission was removed by averaging those output maps which were free from H I emission and subtracting the resultant map from those in which H I was present. Maps of integrated hydrogen emission, radial velocity and velocity dispersion were thus obtained, using a 'gating' procedure to optimize the velocity range for integration (Winter 1975). In some parts of the survey area the velocity profiles were double-

Table 1. Observational details.

Survey parameters				
Map centre	RA	$0^h\ 38^m\ 00^s$		
(1950.0)	dec	$40^o\ 30'\ 00''$		
Mean epoch of survey		1977.5		
Number of spacings observed		121		
Spacing interval		6.1 m		
Smallest spacing		12.2 m		
Largest spacing		737.6 m		
First grating ring radius in RA		2^o		
Primary beam FWHP		94 arcmin		
System noise temperature		120 K		
Continuum receiver				
centre frequency		1422.0 MHz		
bandwidth		10 MHz		
Hydrogen line receiver				
centre frequency		1422.3 MHz		
bandwidth		2 MHz		
velocity coverage		-601 to -192 km/s (heliocentric)		
velocity sampling		13.2 km/s		
velocity resolution		15.8 km/s		
Output map resolution and sensitivity				
Number of spacings included		13	49	121
Angular resolution RA × dec (arcmin)		7.2 × 11.0	1.9 × 2.9	0.8 × 1.2
RMS noise level in 15.8 km/s velocity range (K)		0.1	0.9	3.6
	(mJy)	43	22	14

peaked, and in such cases the velocity and integrated hydrogen associated with each feature were recorded separately. The maps of H I presented here include the emission from both features where found.

The continuum receiver recorded polarized intensity in position angles 0 and 90°, enabling Stokes parameters I and Q to be mapped. No significant emission was found on the map of Q, but the map of total intensity I (with rms noise level 1 mJy) revealed a large number of unresolved sources, all of which were identified with sources from the 5C 3 catalogue (Pooley 1969), including some not previously detected at 21 cm. The positions and flux densities were compared with those in the 5C 3 catalogue and in the survey at 1415 MHz by van der Kruit & Katgert (1972). Positional agreement was found to be within ~ 2–3 arcsec, and the flux density scales agreed to ±5 per cent.

Table 2 gives the position and orientation of M31 and some survey-related parameters. All velocities in this paper are measured relative to the Sun, and map coordinates refer to epoch 1950.0. On contour maps, the synthesized HPBW is represented as a shaded ellipse,

Table 2. Adopted parameters for M31.

Position of optical nucleus (1950.0)	RA $0^h\ 40^m\ 00^s.2$ dec $40^\circ\ 59'\ 43''$	(van der Kruit 1972)
Distance of optical nucleus	690 kpc	(Pellet et al. 1978)
Position angle of major axis	$38^\circ.0$	(Pellet et al. 1978)
Inclination	$77^\circ.5$	(Pellet et al. 1978)
Near side of disc	NW	(Simien et al. 1978)
Systemic velocity	-300 km/s	(Emerson 1976)
Survey-related parameters		
Distance of map centre from nucleus	7.6 kpc	
Primary beam response at nucleus	0.64	
Synthesized beamwidth	160 × 240 pc	
Scale along major axis	1 arcmin = 200 pc	

and the optical nucleus of M31 is indicated by a cross. Where a correction for the primary beam response has been applied, the limit of contouring is at the 40 per cent level.

3 The H I distribution

3.1 INTEGRATED HYDROGEN EMISSION AT 0.8 × 1.2 ARCMIN RESOLUTION

Fig. 1 shows a map of the integrated H I made with the full resolution of the Half-Mile telescope. A number of important features of the hydrogen distribution can be seen in this map:

(i) Almost all the integrated hydrogen brighter than 700 K km s^{-1} lies within a ring between radii of ~ 6.5 and ~ 16 kpc from the nucleus (adopting the parameters from Table 2 for the orientation of the disc). In the region of the nuclear 'bulge' the H I intensity is very low, and no emission from unresolved H I features above the 3σ detection limit of $\sim 8 \times 10^4 M_\odot$/(beam area) was found within 4 kpc of the nucleus. Significant H I outside the ring is detected in only two areas, both of low brightness, and more easily seen on a map made at lower resolution (Section 3.2). One of these features, at RA $0^h\,35^m$, dec $40^\circ\,10'$, joins a concentration of H I at a large distance from the nucleus to the bright ring of hydrogen emission (Newton & Emerson 1977). The other at RA $0^h\,40^m.5$, dec $40^\circ\,35'$, is part of a faint H I arm at a radius ~ 19 kpc.

(ii) The bright ring of H I emission exhibits complex fine structure, and there are many features unresolved by the 0.8 × 1.2 arcmin beam. Plate 1 shows a representation of Fig. 1 as a radio 'photograph' to illustrate the detailed structure. Some weak features can be distinguished at a level below the first contour in Fig. 1. Most of the neutral hydrogen lies in narrow arms up to ~ 600 pc wide which can be traced for up to ~ 6 kpc along their lengths. For reference, the most clearly-defined of these arm segments are shown in Fig. 2 as solid curves on a schematic map of the survey area. The numbering system of Baade (1963) has not been adopted because there is not always a clear correspondence between these 'arms' and the bright spiral arms on optical photographs. Along the H I arms, both the width and intensity change considerably, giving rise to a 'knotty' rather than a smooth appearance.

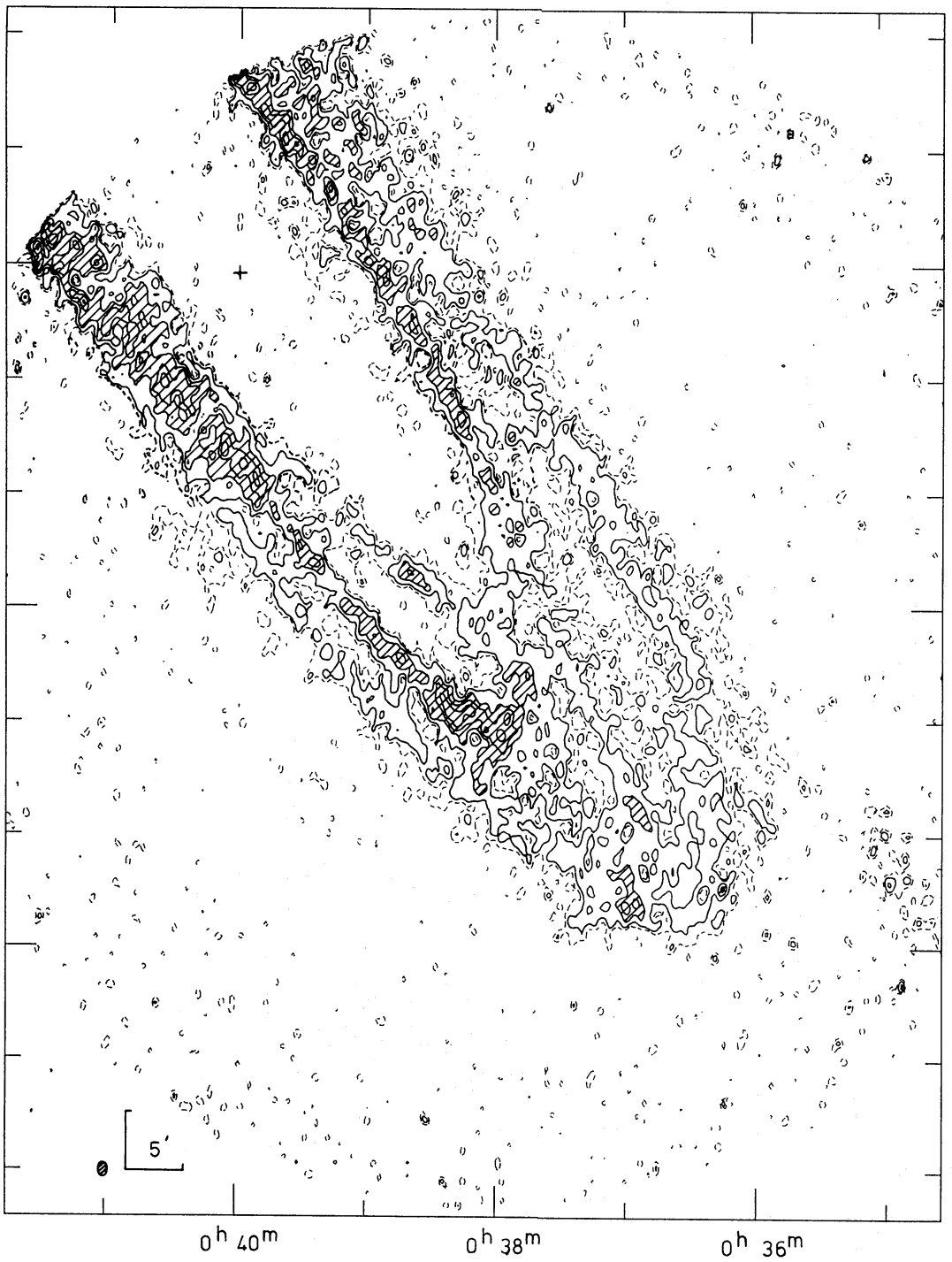

Figure 1. Integrated hydrogen map of the south-west region of M31 at a resolution of 0.8 × 1.2 arcmin. The contour interval is 700 K km s^{-1}, with an additional dashed contour at 300 K km s^{-1}. Regions brighter than 1400 K km s^{-1} are shown shaded. A correction for the primary beam response has been applied; the noise level depends on the number of points included in the integration of each profile, but is typically ~130 K km s^{-1} at the map centre, and rises to 2.5 times this value at the limit of contouring.

These irregularities are greater than those caused by the 'gating' procedure or by noise on the output maps, and closely follow a similar phenomenon in the optical emission (Section 4.1). If the spiral arms of M31 are composed of a series of H I clouds, then a typical cloud must be $\lesssim$ 100 pc in diameter.

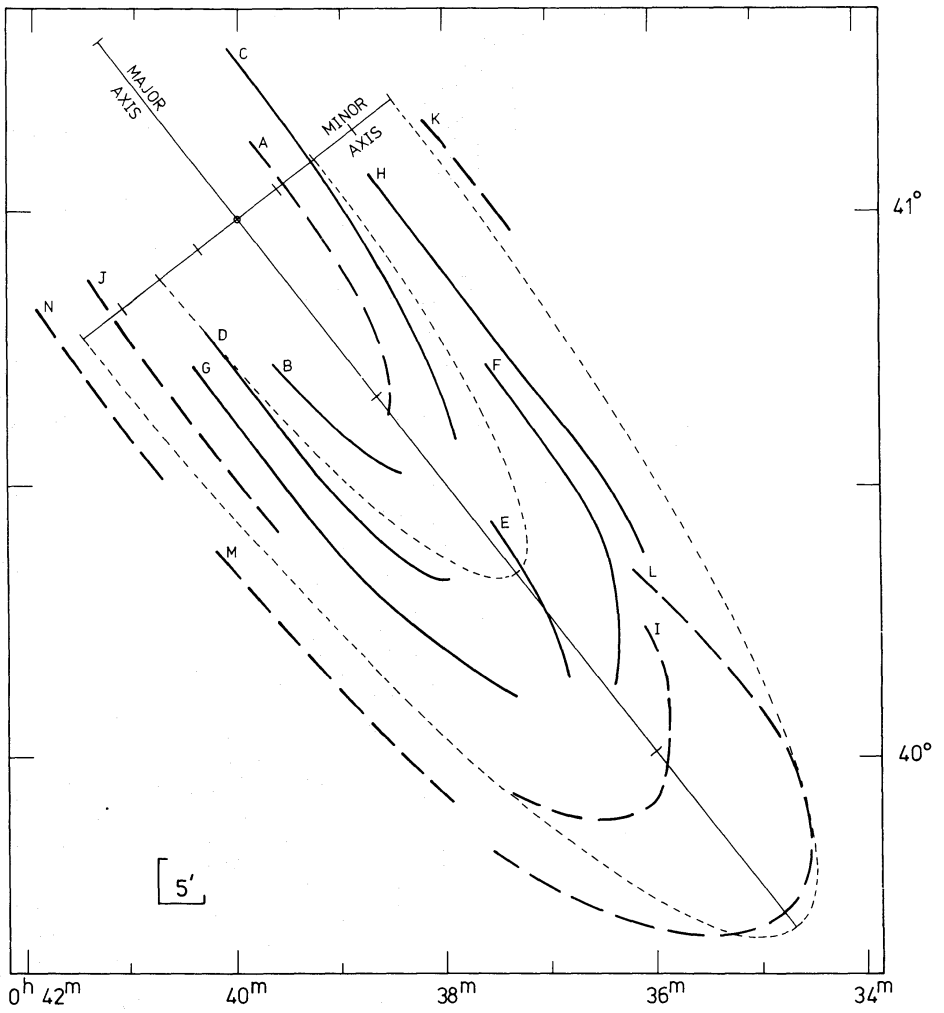

Figure 2. Schematic map of H I arm segments taken from Fig. 1 (solid curves) and from Fig. 4 (dashed curves); each segment is lettered for reference to the text. The major and minor axes of M31 are marked at intervals of 5 kpc, and the dashed semi-ellipses represent distances of 10 and 20 kpc from the nucleus.

(iii) The arm segments in Fig. 1 and Plate 1 become confused in regions near the minor axis due to the combined effects of finite arm thickness and the small inclination of the plane of M31 to the line of sight. Since most of the H I arms are resolved by the telescope beam, this effect is not due to beam smearing, and therefore observations of higher angular resolution are unlikely to separate adjacent arm segments in the region of the minor axis. An arm thickness of 500 pc at a radius of 12 kpc (Emerson 1976) would largely account for the confusion of arms separated by ~4 kpc, if the disc inclination is taken to be 77°.5. However, Plate 1 shows that the arms are more easily separated on the north-west side of the major axis than on the south-east side; in particular, arm *C* (Fig. 2) can be clearly followed across the minor axis. This effect is further illustrated by a cut through the hydrogen distribution along the minor axis (Fig. 3(a)). Since the separation of adjacent arms is very sensitive to the disc inclination, it is possible that the south-east side of the disc is more highly inclined to the line of sight; a warp of ~ 5° could account for the asymmetry observed. A distortion of this sort cannot be produced by a symmetrical warp model (e.g. Newton & Emerson 1977; Henderson 1979).

(iv) Where the H I arms are well separated, a low projected density is found for the gas between them, and the contrast ratio between arm and inter-arm intensities is therefore

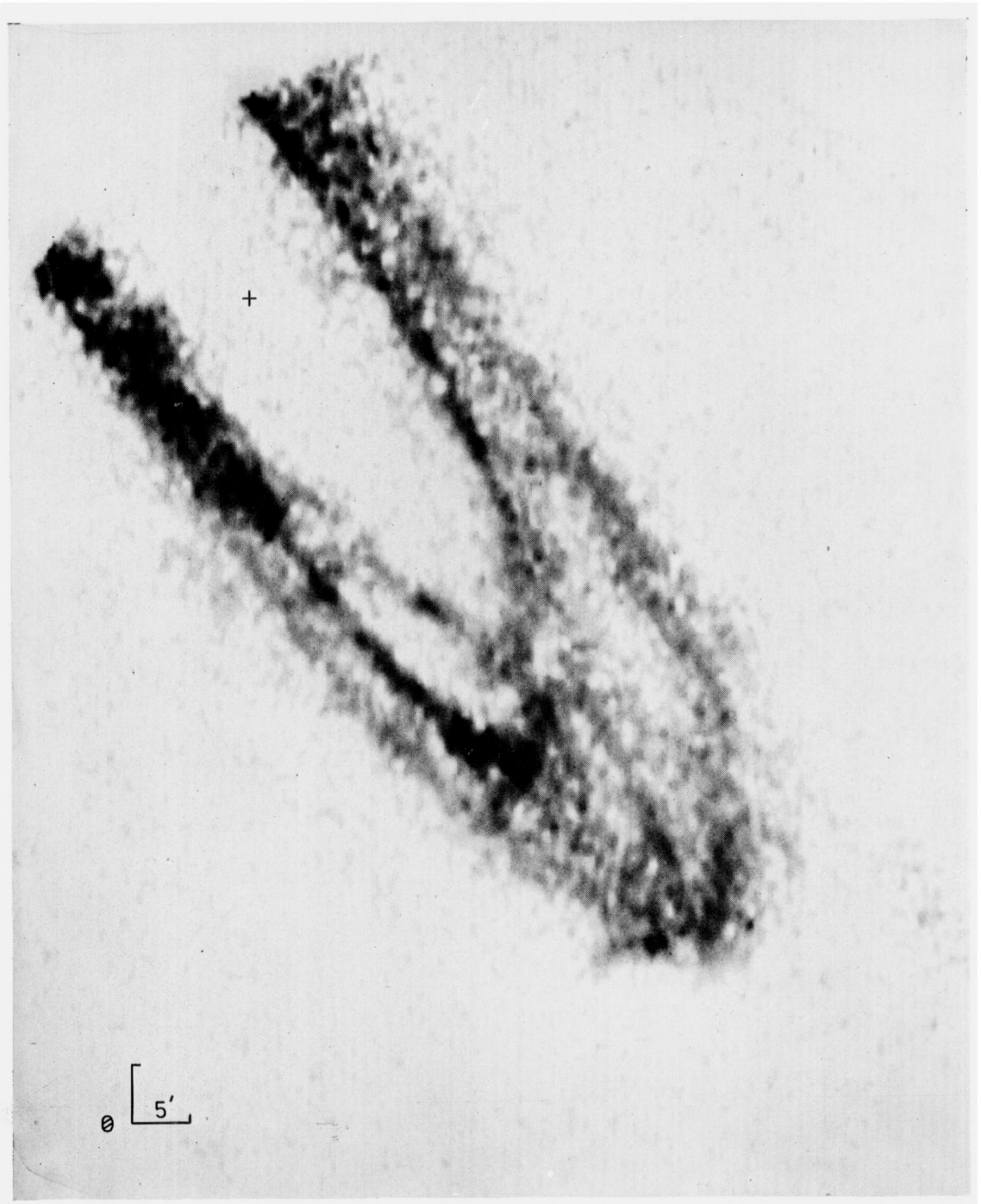

Plate 1. Radio photograph of integrated hydrogen emission in the SW region of M31, at a resolution of 0.8 × 1.2 arcmin.

facing page 556]

Plate 2. Contours of integrated hydrogen emission at a resolution of 0.8×1.2 arcmin superimposed on a Palomar 48-in. Schmidt photograph of M31. The contour interval is 650 K km s^{-1}, with the first contour shown dashed. (Photograph from the Hale Observatories.)

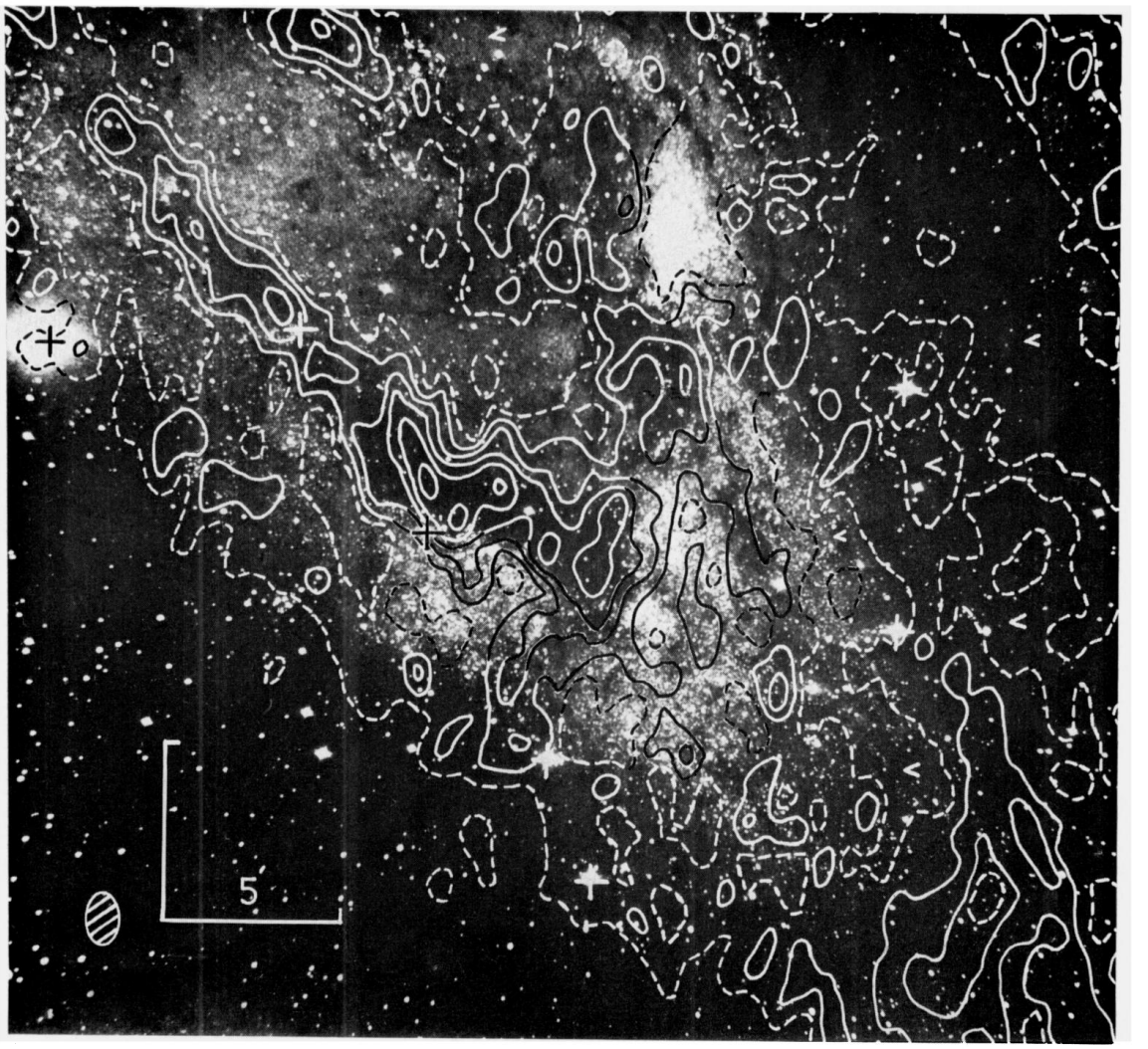

Plate 3. Contours of integrated hydrogen emission at a resolution of 0.8×1.2 arcmin superimposed on a 100-in. Mount Wilson photograph of the SW region of M31. The contour interval is 525 K km s^{-1}, with the first contour shown dashed. (Photograph from the Hale Observatories.)

1980MNRAS.190..551U

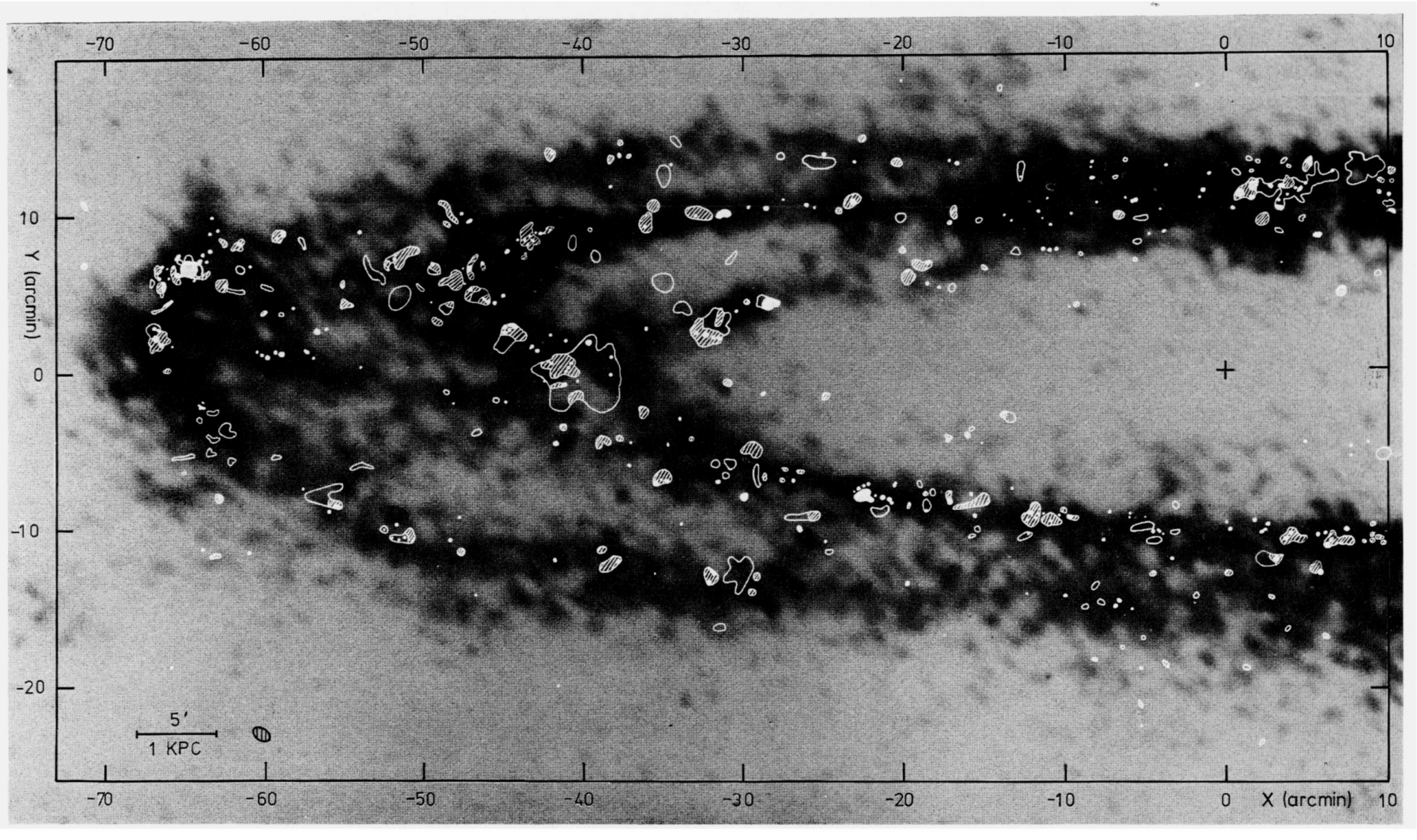

Plate 4. Radio photograph of integrated hydrogen emission in the SW region of M31 with superimposed outlines of H II regions from Pellet *et al.* (1978). Outline, shaded and solid symbols represent H II regions of increasing surface brightness (see Section 4.3).

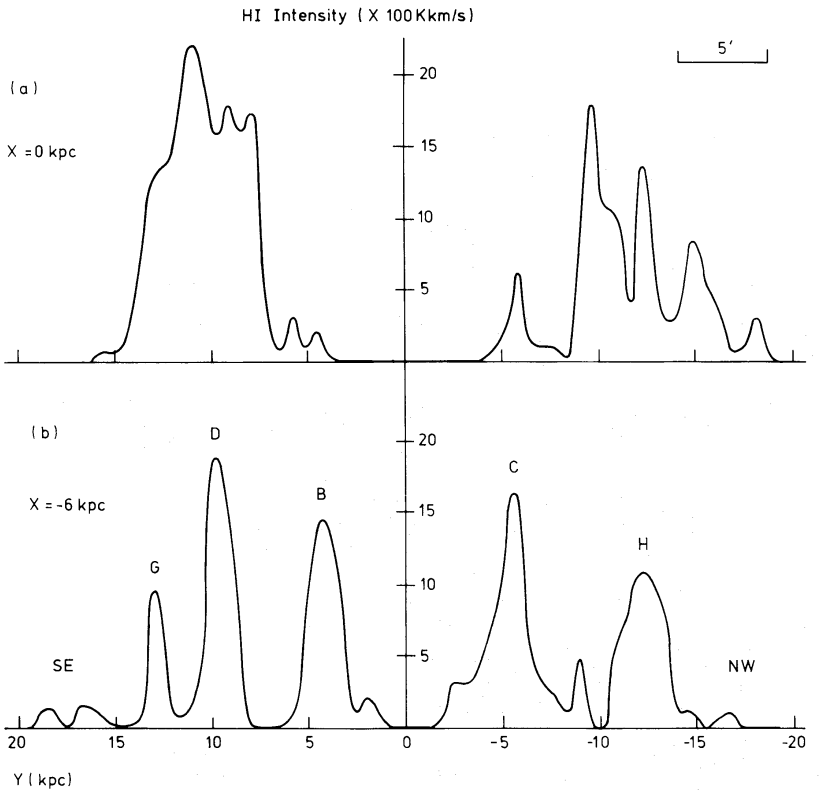

Figure 3. Cuts across the integrated hydrogen map in Fig. 1, (a) along the minor axis, and (b) parallel to the minor axis and displaced 6 kpc to the south-west. X and Y coordinates refer to the major and minor axes respectively, with X increasing along the north-east major axis and Y increasing along the south-east minor axis (Pellet *et al.* 1978).

large; typically it is ~4:1 but reaches ~10:1 along the brightest HI arms (*C* and *D*). Measurement of contrast ratios presents a number of difficulties however. First, low-brightness emission in the minima between some of the arms does not appear on the high-resolution map (Fig. 1), because of the gating procedure used to determine the integrated hydrogen emission. A map made with lower angular resolution is more sensitive to extended low-brightness emission, and enables the HI intensity at these positions to be measured, provided that the minima are resolved at reduced resolution. Fig. 3(b) shows a cut across Fig. 1 parallel to the minor axis, and displaced 6 kpc from it; the five brightest peaks are identified with the arm segments *B*, *C*, *D*, *G* and *H* in Fig. 2. The minimum at $X = -6$ kpc, $Y = 7$ kpc in Fig. 3(b) has an intensity of ~160 K km s^{-1} on an HI map made with a resolution of 1.9 x 2.9 arcmin (Section 3.2), a value typical of the inter-arm regions. Secondly, the absence of structure on scales $\gtrsim 1^\circ$ (Section 2) means that an extended background of HI emission may be present, thereby reducing the true contrast ratio. Thirdly, several spiral arms contain features which are unresolved by the 0.8 x 1.2 arcmin beam, and the peak intensities of these 'knots' may be underestimated. Moreover, since self-absorption may be significant in a few of the brightest features, the largest contrast ratios may be significantly larger than the value of ~10:1 estimated from these observations. In the density-wave theory of spiral structure, the contrast ratio is a measure of the gas compression caused by a spiral potential field (Roberts 1969); an asymmetry is expected in the profile across an HI arm, but the present survey has insufficient angular resolution to detect such an effect.

3.2 INTEGRATED HYDROGEN EMISSION AT 1.9 × 2.9 ARCMIN RESOLUTION

Output maps at 1.9 x 2.9 arcmin resolution were made using observations at 49 spacings, thereby increasing the sensitivity to low-brightness extended emission by a factor ~ 4. Fig. 4 shows a map of integrated hydrogen emission made from these low-resolution output maps. The outer dashed contour in the south-west region of the map was derived from the individual output maps, and is in good agreement with observations of the extreme south-west end of the major axis by Newton & Emerson (1977). A small response due to the

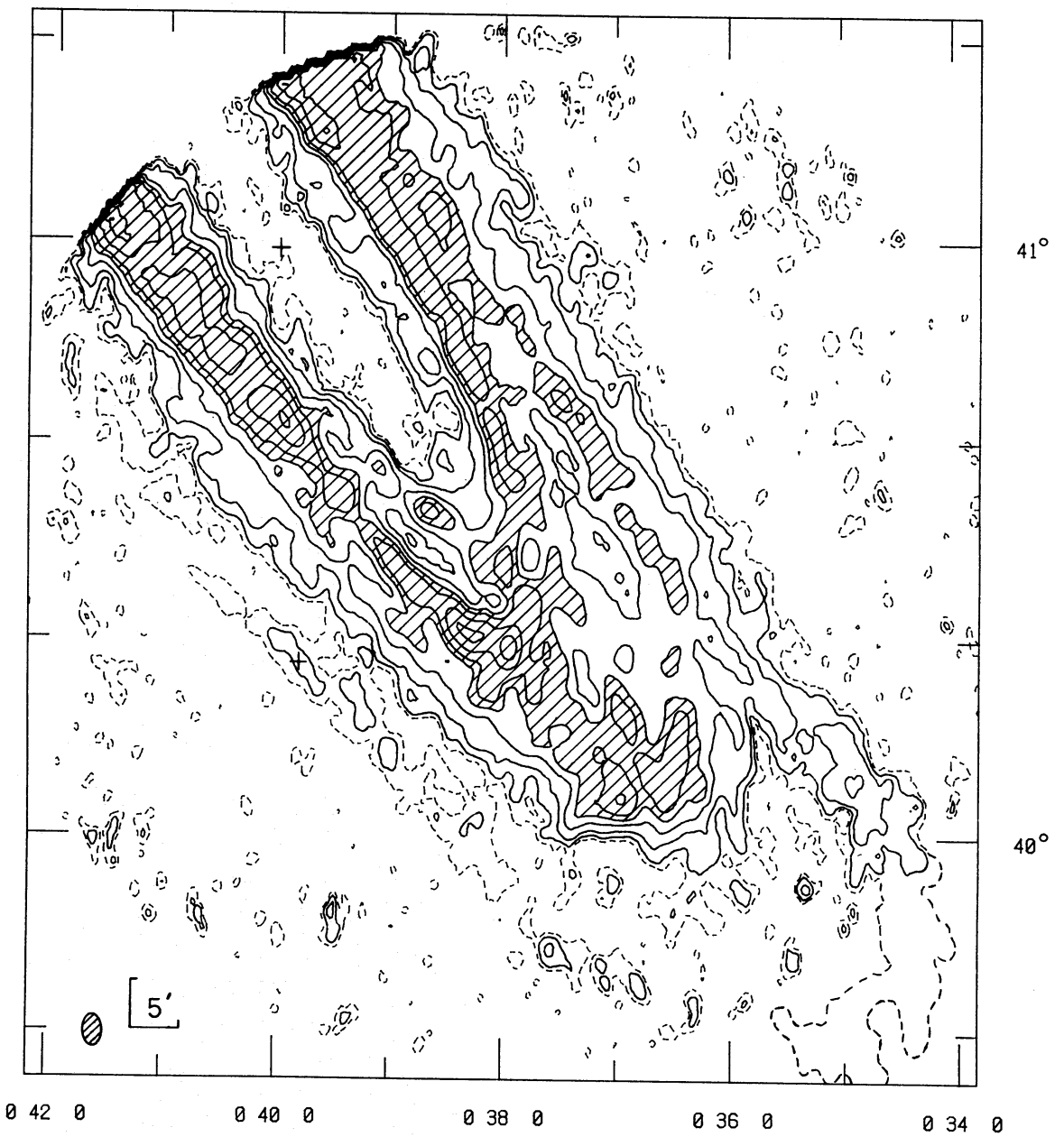

Figure 4. Integrated hydrogen map of the south-west region of M31 made with a synthesized beam of 1.9 × 2.9 arcmin. Solid contours are shown at 150, 300, 600, 900, 1200, 1800 and 2400 K km s^{-1}, with regions brighter than 900 K km s^{-1} shaded. An additional dashed contour at 60 K km s^{-1} is also shown (traced in the extreme south-west from the individual output maps). A correction for the primary beam response has been applied; the noise level at the map centre is ~ 30 K km s^{-1}, rising to 2.5 times this value at the limit of contouring. The position of the star cloud 'Andromeda IV' is marked with a cross.

strong continuum source 4C 39.03 (RA $0^h 39^m.6$, dec $39° 53'$) is visible on this map, due to incomplete continuum removal; the effect of other continuum sources is negligible.

Because of improved sensitivity, H I is detected at greater distances from the nucleus than in Fig. 1, and the outer radius of the 'ring' of bright H I emission is increased to ~ 19 kpc. Many of the arm segments visible in Fig. 1 are confused in Fig. 4, but beyond radii ~ 19 kpc some further H I arm segments are visible, and these are well separated despite the increase in beam size. They have been added to Fig. 2 as dashed curves (*I*, *J*, *K*, *L*, *M* and *N*). Arm *L* can be traced eastwards beyond its crossing of the major axis, and it appears to be continuous with arm *M*, and possibly also arm *N*. A peak of extended emission has been detected at RA $0^h 34^m$, dec $39° 30'$ by Newton & Emerson (1977, Fig. 1), and is probably associated with an outer arm which crosses the major axis at a radius ~ 24 kpc, rather than with arm *L*.

The innermost arm detected in H I is arm *A*, which is coincident with a prominent dust lane at a radius ~ 5 kpc. It is just detetcted at a few points along its length at a resolution of 0.8 x 1.2 arcmin (Plate 1), and is visible as a 'shoulder' of brightness ~ 300 K km s^{-1} on the inside of arm *C* in Fig. 4. On the north-east side of the minor axis, the radial velocities of the hydrogen in arm *A* are anomalous (Shane 1975a; Emerson 1976), so that it is well separated from arm *C* in maps made using a limited velocity range, even at 1.9 x 2.9 arcmin resolution. Fig. 5 shows a map of H I emission in this region, integrated over a velocity range chosen to illustrate the separation of arms *A* and *C*. The H I cloud at RA $0^h 39^m.7$, dec $41° 04'$ is the brightest part of arm *A*, and is identified with feature (c) detected by Emerson (1976). It has an H I mass ~ $10^6 M_\odot$ and radial velocity -255 ± 5 km s^{-1}, more than 40 km s^{-1} different from the expected value at that position; the large dispersion (110 km s^{-1}) reported by Emerson is not confirmed, and may have resulted from inclusion of H I with 'normal' velocities. The 'anomalous' velocities and the dynamics of this inner H I arm will be discussed in a subsequent paper.

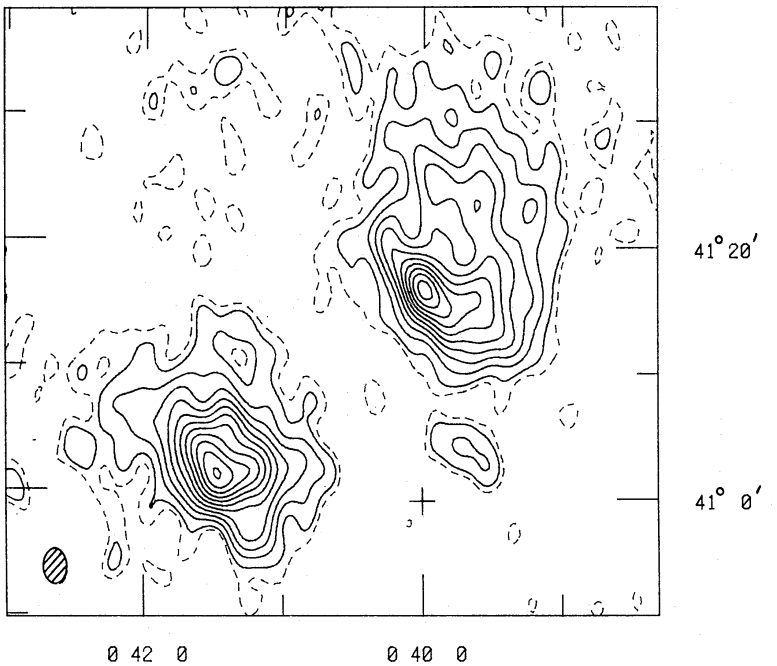

Figure 5. Map of H I emission near the nucleus of M31, integrated over the velocity range -245 to -271 km s^{-1}, at a resolution of 1.9 x 2.9 arcmin. No primary beam correction has been applied; the contour interval is 125 K km s^{-1} at the nucleus, with an additional dashed contour at 62.5 K km s^{-1}.

Within the region of the central bulge the H I intensity is very low but, because of uncertainties in the zero-levels of the output maps (Section 2), areas of extended low-brightness emission would not be detected. However, the innermost 60 K km s^{-1} contour in Fig. 4 shows some emission 2.5 arcmin south of the nucleus. This feature is a marginal detection, with an H I mass of $(2.5 \pm 1.0) \times 10^5 M_\odot$ and a radial velocity of -350 ± 3 km s^{-1}; it may be associated with feature (a) detected by Emerson (1976).

3.3 SPIN TEMPERATURE OF THE NEUTRAL HYDROGEN GAS

Measurement of the absorption of continuum radiation from a source lying behind the disc of M31 provides a means of determining the optical depth $\tau(V)$, and hence the spin temperature T_s of the absorbing gas. Absorption profiles have been obtained for the four brightest unresolved continuum sources in the surface area, but significant absorption was found for only one of these (5C 3.107). The other sources provide the following (2σ) upper limits to the optical depth in a 16 km s^{-1} velocity range along their respective lines of sight:

Source	τ	RA (1950.0)	dec (1950.0)
		h m s	° ′ ″
5C 3.50	<0.23	0 35 41.5	41 20 38
5C 3.106	<0.07	0 39 33.7	39 53 22
5C 3.124	<0.28	0 41 10.1	40 30 09

No H I emission was detected near any of these sources, and therefore no constraint may be placed on the spin temperature of any low-brightness gas in their respective directions.

The powerful continuum source 5C 3.107 lies in a region of bright H I emission, with integrated brightness reaching ~ 2500 K km s^{-1} within 2 arcmin of it. Fig. 6 shows the absorption profile normalized according to the flux measured from the broad-band continuum map; also shown is the emission profile at that position, estimated from profiles within ~ 1 arcmin of it. An absorption of 20 ± 8 per cent is present in the profile at -272 ± 4 km s^{-1}, with a width of 17 ± 3 km s^{-1} (allowing for instrumental broadening). This is a significant result, because Fig. 6 shows that the velocity of the absorption feature is in excellent agreement with that of the emission feature at the same position; Fig. 1 shows that the H I structure changes considerably on scales ~ HPBW at the position of 5C 3.107 (RA 0^h 39^m 34^s.49,

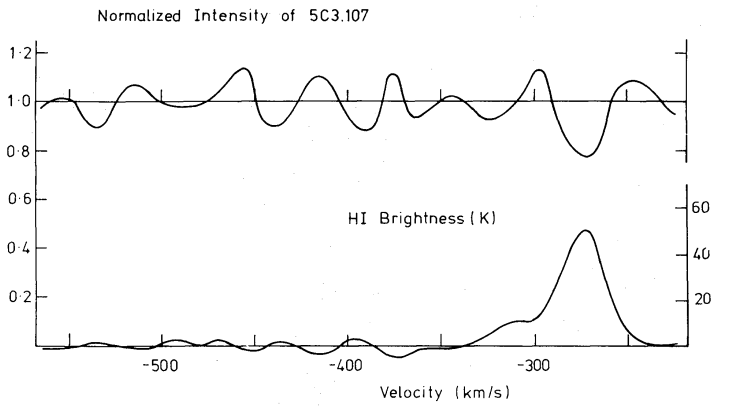

Figure 6. Absorption and emission profiles in the direction of the continuum source 5C 3.107. The absorption profile has been normalized using the flux derived from the broad-band continuum map, and the brightness scale on the emission profile has been corrected for primary beam attenuation.

dec 41° 13′ 00″.1 as measured by the 5-km telescope at 2.7 GHz); the estimated error in the percentage absorption is therefore mainly determined by uncertainties in the 'expected profile' at the same position. Since the absorption feature is resolved in velocity, it is unlikely that finite instrumental resolution has caused an underestimation of its depth.

A spin temperature for the H I gas can be derived only if the continuum source lies beyond the disc of M31; the following information suggests that 5C 3.107 is probably an unrelated background source:

(i) It is unresolved by the 5-km telescope at 2.7 GHz, placing an upper limit of ~ 2 pc on its linear extent, if it lies in the disc of M31. For such a source, the radio luminosity is very large ($P_{1422} \simeq 2 \times 10^{18}$ W Hz^{-1} sr^{-1}), exceeding that of any known compact source in our Galaxy. It is possible that the source could be a young supernova remnant in M31, although its luminosity would be $\gtrsim 10$ times that of Cas A. The only known supernova remnant of comparable radio power was SN1970g in the giant spiral galaxy M101, whose 21-cm luminosity exceeded that of 5C 3.107 for a period ~ 2 yr (Marscher & Brown 1978).

(ii) Table 3 shows the results of flux density measurements made between 1966 and 1978. The flux scales of the 1966, 1970, 1971 and 1977 surveys were made to coincide for 11 strong sources in common to them. There are no variations in the radio luminosity of 5C 3.107 over 11 yr of more than about 5 per cent.

(iii) The source is not optically identified. This is not surprising, because of the brightness of the M31 disc and the visual extinction $A_V (\simeq 3.0 \times E(B-V))$ of ~ 2 mag, if a gas-to-dust ratio of 3.3×10^{21} atom cm^{-2} mag^{-1} is adopted for this line-of-sight (Bajaja & Gergely 1977).

Assuming that 5C 3.107 lies beyond the disc of M31, the measured absorption of 20 per cent implies that the H I gas along the line-of-sight has an optical depth $\tau = 0.22 \pm 0.10$ at a radial velocity of -272 km s^{-1}. The emission brightness temperature $T_b \simeq 50$ K therefore implies that the mean spin temperature is $T_s \simeq 220$ K, with a 1σ uncertainty range from 160 to 420 K. As the line-of-sight to 5C 3.107 may pass through about 2 kpc of disc material, several H I clouds with different temperatures are probably involved. A temperature $T_s \simeq 220$ K is much hotter than that of the cold, dense clouds in the galaxy, but rather cooler than the diffuse inter-cloud medium. The present observations do not have sufficient sensitivity or velocity resolution to separate the effects of hot and cold clouds by means of profile widths.

Integrated brightness temperatures may be converted to surface densities of H I gas by using the well-known relation

$$N_{HI} = 1.823 \times 10^{18} \int T_b(V) dV \text{ atom cm}^{-2}. \quad (1)$$

Table 3. Flux density measurements of 5C 3.107.

Date	Frequency (MHz)	Flux (mJy)	Reference
1966	1407	423 ± 45[1]	Gillespie (1974)
1970	1421	393 ± 20	Gillespie (1974)
1971	1415	390 ± 15	van der Kruit & Katgert (1972)
1972	2695	205 ± 10	Spenser & Burke (1975)
1977	1421	420 ± 10	This paper
1978	2694	185 ± 10	This paper

[1] 5C3 flux (Pooley 1969) revised by Gillespie

If self-absorption is important, then this relation underestimates the true column density of gas by a fraction $\sim \tau/2$ (for small τ). Examination of the output maps to determine peak brightness temperatures gives an indication of whether such effects are likely to be significant elsewhere in the disc of M31. 5C 3.107 lies in one of the few regions where the brightness temperature (in a 16 km s^{-1} velocity range) exceeds 50 K; if a value of $T_s \simeq 220$ K is adopted for the whole disc then the uncertainty in the use of equation (1) is at most 10 per cent. A map of integrated H I brightness is therefore a good representation of the column density of gas projected on to the plane of the sky. Except for a discussion in Section 4.1 of a small region where brightness temperatures $\gtrsim 80$ K are found, the effects of self-absorption are disregarded in this paper.

4 The relation of H I to other Population I material

4.1 H I AND OPTICAL EMISSION

Plate 2 shows a contour map of integrated H I emission superimposed on a 48-in. Schmidt photograph of M31; positional alignment is to within ~ 10 arcsec over most of the map area. A very close correlation exists between H I emission and dust features, and many of the irregularities in the H I distribution correspond exactly with the patchy appearance of the dust lanes. In particular, the well-defined H I arm segments, *B*, *C*, *D*, *E* and *F* (Fig. 2) lie *along* narrow dust lanes, with no relative displacement. The correlation can be seen in more detail in Plate 3, which shows a 100-in. Mount Wilson photograph of an area near the centre of the survey, with overlaid contours of H I emission. The scale size of the correlation is limited by the angular resolution of the H I map, rather than by sensitivity; since the beam size is 160 × 240 pc, gas and dust are evidently well mixed on scales $\lesssim 100$ pc. Variations in integrated H I emission along an arm segment follow changes in the darkness of the corresponding dust features; this is particularly evident along arms *B* and *D* (Plate 2), demonstrating the correlation of gas and dust along the line-of-sight. These results confirm the earlier work of Emerson (1974), who examined the correlation with dust using an H I map made with a beam size of 320 × 480 pc.

Plate 2 shows one striking exception to the excellent overall correlation between H I gas and dust: the prominent dust lane on the north-west side of the nuclear bulge (at a radius ~ 6 kpc) has very little H I associated with it. This is probably due to a combination of two effects. First, the mass of dust involved may be small, since the dust lane is silhouetted against the bright nuclear bulge (Emerson 1974). Secondly, the gas-to-dust ratio is a function of distance from the nucleus (Bajaja & Gergely 1977): between radii of 10 and 20 kpc its value is roughly twice that for radii < 10 kpc. The weak H I arm segment *A* lies along this dust lane, and its low H I intensity of ~ 300 K km s^{-1} (Fig. 4) therefore reflects a decrease in the gas-to-dust ratio for the inner parts of the disc.

The darkest dust clouds in the south of M31, and also the most intense H I emission are found at the southern end of arm segment *D* (Plate 3), where the integrated brightness reaches 3350 K km s^{-1}. H I brightness temperatures of up to 84 K are found in arm *D*, and it is likely that self-absorption is significant; if a spin temperature $T_s \sim 120$ K is adopted for the H I gas, then the H I column density is underestimated by a factor ≈ 1.6. The visual extinction at this position is very large, and a gas-to-dust ratio of 4×10^{21} atom cm^{-2} mag^{-1} (Bajaja & Gergely 1977) yields a value of $A_v \sim 6$. Van den Bergh (1964) has noted that the boundaries of some of the OB associations which lie near the outer edge of arm *D* are determined by absorption, and this estimate of A_v confirms that the optical appearance of the disc is strongly affected by obscuration.

4.2 HI AND OB ASSOCIATIONS

Fig. 7 shows an integrated HI map of the survey area with superposed outlines of OB associations from van den Bergh (1964), who classified them as young, intermediate or old according to the degree of subclustering within each association. The synthesized HI beam is

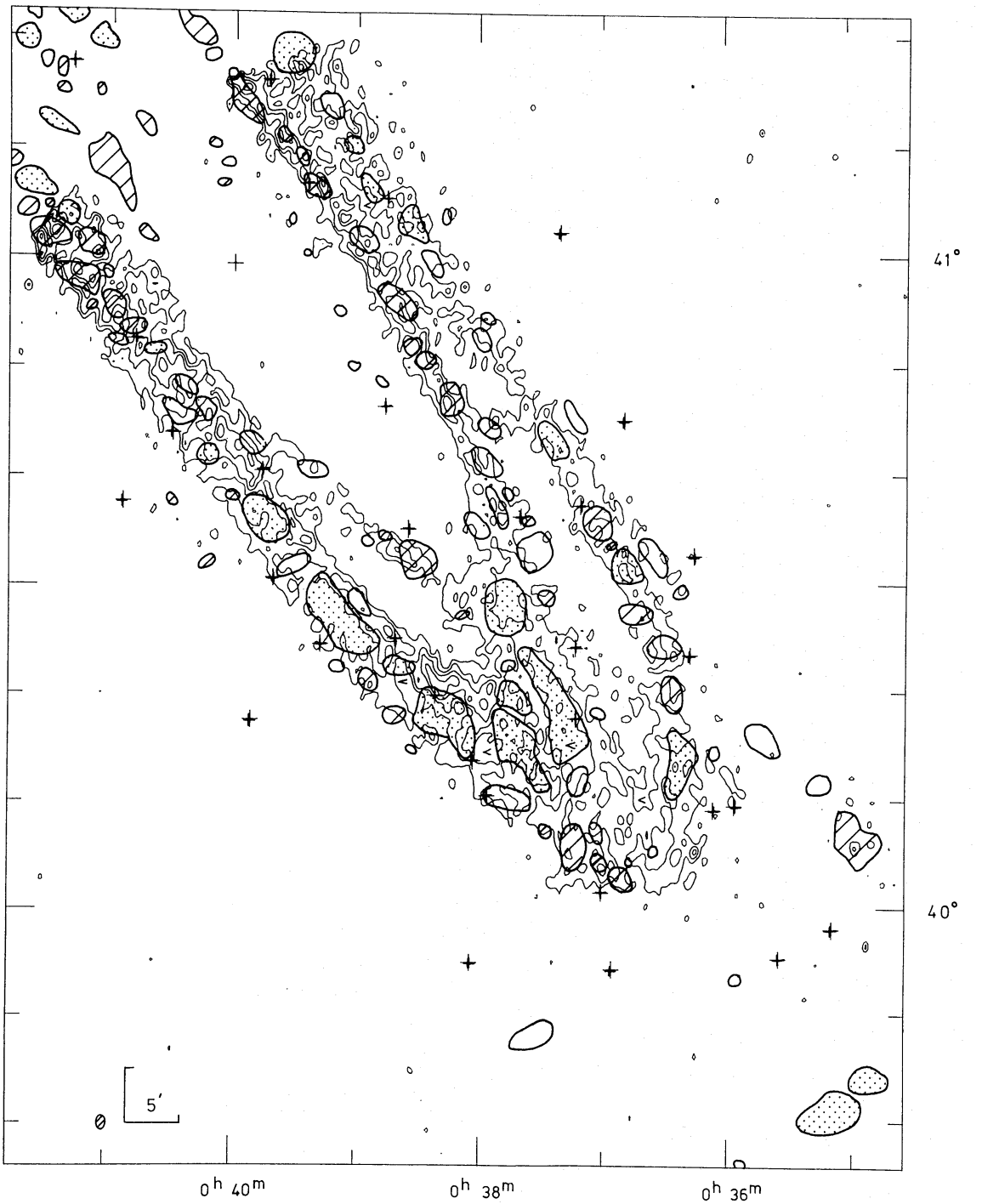

Figure 7. Integrated hydrogen map of the south-west region of M31 at a resolution of 0.8 × 1.2 arcmin, with superimposed outlines of OB associations from van den Bergh (1964). The contour interval is 700 K km s^{-1}, and shading within the associations indicates their age: cross-hatched, young; dotted, intermediate or old; no shading, unclassified.

160 x 240 pc, comparable with the size of the smallest OB associations; a detailed comparison with the distribution of H I gas can therefore be made.

There is excellent agreement between the large-scale distributions of H I and OB associations, implying that there is a broad correlation between neutral hydrogen gas and young Population I stars on scales $\gtrsim 2$ kpc. Very few associations are found beyond the limit of bright H I emission (~ 16 kpc from the nucleus); on the lower resolution H I map (Fig. 4) most of these were found to lie along the outer H I arm segment *L*. In fact, only one association within the present survey area (OB12 in the notation of van den Bergh 1964) does not have H I emission brighter than 60 K km s^{-1} within its outline. This association is only 3 kpc from the nucleus, and lies inside the extended central deficiency of neutral hydrogen. Van den Bergh (1972) found the old star cloud 'Andromeda IV' whilst searching for possible dwarf companion galaxies to M31; it is marked with a cross in Fig. 4 at RA $0^h 39^m.8$, dec $40° 18'$ and appears to be associated with the outer H I arm segment *M*.

A detailed comparison of distributions of H I and OB associations reveals that the relation between them is different for the two sides of the major axis:

(i) On the north-west side of the major axis the associations lie along strings at radii ~ 9 kpc and ~ 15 kpc from the nucleus, and are clearly correlated with H I arm segments on scales of a few arcmin. The innermost of these strings comprises mainly young associations, and closely follows the H I arm segment *C*, with a slight tendency for the OB associations to lie at larger radii than the H I arm; the outer string of associations traces the H I arm segments *F* and *H*.

(ii) Many of the associations on the south-east side of the major axis tend to avoid peaks of H I emission. In particular the string of mainly old and intermediate-age associations which comprise the bright optical arm S4 (Baade 1963) lies in an extended minimum of H I emission *between* the well-defined H I arm segments *D* and *G* (Plate 1).

These differences may be explained on the following assumption: (a) the north-west side of the disc is the near side of M31; (b) the gas and dust are well mixed on scales $\lesssim 150$ pc; (c) the gas and OB associations extend to $\pm \sim 150$ pc from the plane of M31; (d) the gas and dust lie on the inside edges of bright spiral arms.

On the south-east side of the major axis, the gas and dust appear in front of the bright stellar associations, and their inner edges are therefore obscured by several magnitudes of visual extinction (Section 4.1), with dust lanes forming their inner boundaries. Fig. 7 shows that the OB associations which outline Baade's arm S4 are bounded on their inside edges by the H I arm segment *D*, and a disc thickness of ~ 300 pc is sufficient to account for the observed effect. On the near (north-west) side of the major axis, H I gas and dust lie behind the OB associations, and consequently dust has little effect on the boundaries of the associations. The slight shift between the H I arm segment *C* and its corresponding string of OB associations therefore represents a real displacement between them in the plane of the galaxy of ~ 1 kpc. This conclusion is supported by the visual appearance of these associations (OB61–72): van den Bergh (1964) has noted that most of them lie close to absorption lanes or are surrounded by them, but that few of these associations have their boundaries determined by dust.

The spiral arm which comprises the H I arm segment *D* and the string of associations which trace Baade's arm S4 shows some evidence for an age gradient across it. Van den Bergh (1964) found that, within the associations OB81 and OB82, subclustering of OB stars is mostly concentrated near their inner edges, suggesting an age gradient as a function of radius. A number of the associations in this arm are bounded on their inner edges by a dark dust lane, along which runs the well-defined H I arm *D* (Plate 3). Because H I and dust have been shown to be closely correlated, it is likely that the youngest parts of these associations

(mainly of intermediate age) are obscured by dust. Star formation is currently taking place in these obscured areas, as a narrow string of H II regions is found to run along the H I arm *D* (Section 4.3). If the spiral arms are assumed to be trailing, and to lie within the corotation radius, then these results are in qualitative agreement with the predictions of the density-wave theory of spiral structure (Roberts 1969); the youngest Population I material (H I gas and H II regions) is expected to lie on the inside edges of broad stellar arms in this case. However, the corotation radius is unknown, and the sense of winding of the spiral arms is not clear (Section 5), so this cannot be regarded as strong evidence in favour of the density-wave theory.

4.3 NEUTRAL HYDROGEN AND H II REGIONS

The most sensitive survey of H II regions in M31 is that by Pellet *et al.* (1978) who produced a catalogue giving positions, dimensions and surface brightness of 981 H II regions, many of which are extended. Plate 4 shows a radio photograph of the survey area with a map of H II regions from Pellet *et al.* superimposed. Within the outline of each H II region, shading indicates the surface brightness in the Hα line according to the following scale:

solid	$S > 3.0$	($\times 10^{-5}$ erg s^{-1} cm^{-2} sr^{-1})
shaded	$3.0 > S > 1.0$	
outline	$1.0 > S > 0.35$	(detection limit).

The X, Y coordinates in Plate 4 are explained in the caption to Fig. 3; alignment of the H I and Hα surveys is better than 15 arcsec over the whole map area.

There is a striking correlation between the distributions of H I gas and H II regions on both large and small scales. Almost all the H II regions lie in the same ring to which the H I is largely confined; very few are found in the innermost 5 kpc where the H I intensity is low, or beyond a radius of 15 kpc. In detail, the H II regions show a clear tendency to lie in strings along H I arm segments, and to avoid the inter-arm areas of low H I brightness. In contrast with the distribution of OB associations, there is no detectable asymmetry between the two sides of the major axis; wherever the arms traced in H I and H II regions are both clearly defined, no relative displacement is found, and therefore H II regions and H I gas must co-exist on scales of ~ the 21-cm beam-size.

The tendency for H II regions to be found in areas of bright H I emission can be quantified by studying the correlation between their respective surface densities. A region of the galaxy bounded by the minor axis and a semicircle of radius 20 kpc was selected for this purpose; 414 H I regions from the catalogue of Pellet *et al.* (1978) lie within this area, in which the primary beam response is >50 per cent. The surface density of H II regions σ_{HII} was determined (in intervals of H I intensity σ_{HI}), by evaluating the average number of H II regions per unit area over regions of the disc where σ_{HI} lay in the given interval. This method therefore differs from that used by Berkhuijsen (1977) to generate regression line p1, since no smoothing of the H II region data has been applied. A few very extended H II regions, to which no unique value of σ_{HI} could be assigned, were excluded from the analysis. Fig. 8(a) shows the variation of σ_{HII} with σ_{HI} plotted on logarithmic scales. The gating procedure used to evaluate the σ_{HI} causes the mean H I intensity in areas of low brightness to be underestimated; this has a significant effect only on the point plotted at 150 K km s^{-1} in Fig. 8(a), which may be in error by $\lesssim 100$ K km s^{-1}. It is clear that σ_{HII} and σ_{HI} are highly correlated, and that a power-law relation of the form $\sigma_{HII} \propto \sigma_{HI}^{n}$ is a good fit to the data for values of $\sigma_{HI} \lesssim 2000$ K km s^{-1}. A weighted least-squares slope of $n = 1.37 \pm 0.07$ was obtained, rather less than the value of $n = 2.23 \pm 0.11$ found by Emerson (1974), who used an H I map with

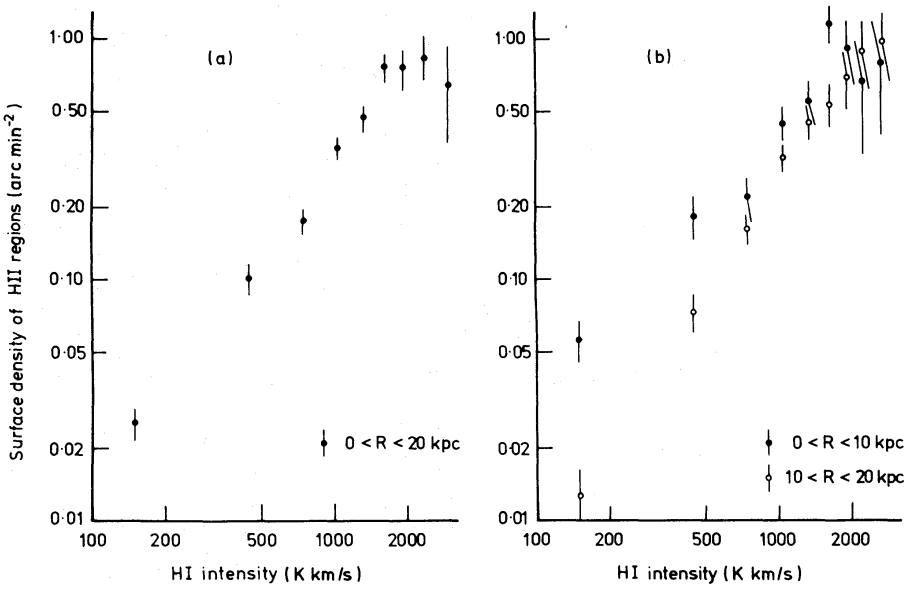

Figure 8. Variation of surface density of H II regions σ_{HII} from Pellet *et al.* (1978) with integrated H I brightness σ_{HI} for the south-west side of the minor axis of M31. (a) Radii up to 20 kpc from the nucleus. (b) Filled circles: radii up to 10 kpc; open circles: radii between 10 and 20 kpc. Vertical bars indicate the estimated uncertainty in σ_{HII}.

resolution 1.5 x 2.2 arcmin and data on H II regions from Baade & Arp (1964). The analysis was repeated using the catalogue of Baade & Arp; it yielded a value of $n = 1.5 \pm 0.1$, demonstrating that the difference lies in the H I maps rather than in the H II regions. Table 4 (lines 1–5) shows the results of determinations of n using H I data made with four angular resolutions, and it is evident that larger values of n are found when low-resolution maps are used. The result of Berkhuijsen (1977) is not directly comparable with the others, because of the different method of analysis used. Interpretations of the index value n must take account of the respective scale-sizes over which the optical and radio data are averaged. Since an extended component of H I emission may be missing from these observations (Section 2),

Table 4. Relation between surface densities of H II regions and H I gas.

Index n defined by $\sigma_{HII} \propto \sigma_{HI}^{n}$

HI beam size (arcmin)	n	standard error	HII region survey	Reference
0.8 × 1.2	1.37	0.07	Pellet et al. (1978)	This paper
0.8 × 1.2	1.50	0.10	Baade & Arp (1964)	This paper
1.5 × 2.2	2.23	0.11	Baade & Arp (1964)	Emerson (1974)
4.8 × 4.8	1.97	0.20	Baade & Arp (1964)*	Berkhuijsen (1977)
10 × 11	3.50	0.14	Baade & Arp (1964)	Hartwick (1971)
0.8 × 1.2 (R < 10 kpc)	1.17	0.13	Pellet et al. (1978)	This paper
0.8 × 1.2 (10 < R < 20 kpc)	1.54	0.06	Pellet et al. (1978)	This paper

*Data smoothed to a resolution of 4.8 × 4.8 arcmin.

it is possible that σ_{HI} is underestimated. Whilst this effect tends to reduce the measured value of n, it is insufficient to account for the differences noted above. H I observations of higher angular resolution might reveal a smaller value of n than the value of 1.37 derived here, although allowance would have to be made for the finite angular extent of many of the H II regions catalogued by Pellet *et al.* (1978); this is not believed to have a significant effect on the present analysis.

Fig. 8(a) shows that in areas where the H I intensity is $\gtrsim 2000\,\mathrm{K\,km\,s^{-1}}$ the surface density of H II regions is less than would be expected from an extrapolation of the power-law relation appropriate for small intensities. This 'saturation' effect has been noted by Emerson (1974) for regions of M31 with H I intensity $\gtrsim 3000\,\mathrm{K\,km\,s^{-1}}$, and by Newton (1978) for the inner parts of M33. It is most likely to be due to obscuration of the emission from H II regions by dust, known to be highly correlated with H I gas, especially where the H I column density is large. H II regions therefore tend to cluster *around* the brightest peaks of H I emission, as can be seen in Fig. 9, an H I contour map of a small area near the centre of the region covered by Plate 3. The bright H I emission comes from the southern end of arm segment D, and the H II regions (from Pellet *et al.* 1978) generally lie on an H I gradient, rather than on the peak of this arm. Plate 3 shows that these H II regions lie on the outer edge of the dark dust lane which follows arm D, and it is therefore likely that a number have escaped detection in this small area. Elsewhere along arm D (e.g. near $X = -30$ arcmin, $Y = 10$ arcmin in Plate 4), the H I gas is less bright and these effects are not apparent. If a power-law relation between σ_{HII} and σ_{HI} is in fact appropriate even at large H I intensities (in the absence of dust), then about 80 H II regions from the catalogue of Pellet *et al.* (1978) are missing because of obscuration.

A possible radial variation in the relation between σ_{HII} and σ_{HI} was investigated by analysing the inner and outer parts of the galaxy separately. Fig. 8(b) shows that there are considerable differences for radii < 10 and > 10 kpc, and a significant difference in the

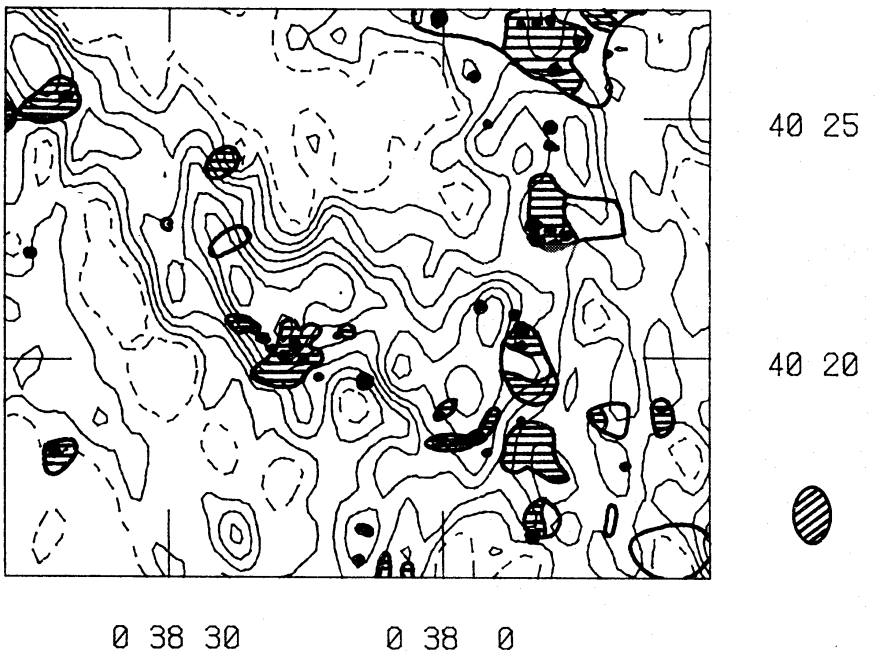

Figure 9. Integrated hydrogen map of a small area of M31 near the centre of the survey, with superimposed outlines of H II regions from Pellet *et al.* (1978). The contour interval is $400\,\mathrm{K\,km\,s^{-1}}$, with the first contour shown dashed. Outline, shaded and solid symbols represent H II regions of increasing surface brightness (see Section 4.3).

weighted least-squares slope n was found (Table 4, lines 6 and 7). Whilst systematic effects due to missing extended H I emission (Section 2) could affect the index n differently, they are not large enough to explain the change in n between the inner and outer parts of the disc. The results imply that in regions of low H I density, formation of H II regions is more efficient in the inner parts of the galaxy.

A number of 'bubble-like' H II regions were found by Pellet *et al.* (1978), 12 of which lie in the present survey area. As with H II regions in general, they tend to be in areas of bright H I emission. If these regions represent a late stage in the life of an expanding ionized region, then disturbances might be expected in the surrounding H I emission. No distinctive H I features were found near these bubble-like regions, several of which lay on the well-defined ridges which make up the spiral arm segments. Only one H II region (no. 323 in the catalogue of Pellet *et al.*, and not bubble-like) is found in a conspicuous minimum of H I emission. It lies within the young OB association OB67 which fills a 'hole' in the H I arm *C* at RA $0^h\,38^m.5$, dec $40°\,52'$ (Fig. 7), and is clearly visible in Plate 1. H I gas appears to have been consumed within this association, presumably by ionization.

The bright OB association OB78 (=NGC 206) at RA $0^h\,37^m.8$, dec $40°\,29'$ (Fig. 7) provides evidence that ionization may have a significant effect on the H I morphology elsewhere also. This association is bounded on three sides by H I emission $\gtrsim 700\,\mathrm{K\,km\,s^{-1}}$, but very little H I is found within its outline (Plate 3). Largely coincident with it is an extended area of low-brightness Hα emission (no. 184 in Pellet *et al.* 1978), with emission measure $EM \gtrsim 40\,\mathrm{cm^{-6}\,pc}$. For a known thickness D of the emitting region, the column density $N_{\mathrm{HII}} = (EM \times D)^{1/2}$ of ionized hydrogen can be calculated. The values $D \sim 2$ kpc (H I disc thickness x cosec inclination) and $EM = 40\,\mathrm{cm^{-6}\,pc}$ lead to $N_{\mathrm{HII}} \simeq 8.7 \times 10^{20}\,\mathrm{cm^{-2}}$, and an average electron density $\simeq 0.14\,\mathrm{cm^{-3}}$. The H I morphology suggests that H I gas has been ionized within this association, and the integrated H I brightness of a column of gas with surface density N_{HII} is $\sim 480\,\mathrm{K\,km\,s^{-1}}$, comparable with the contour interval in Plate 3. A large number of young, hot OB stars are present in this rich association, and van den Bergh (1966) has found $\gtrsim 300$ stars brighter than $B = 21.0$, corresponding to spectral types earlier than B0; it therefore seems probable that these provide the ultraviolet radiation required to ionize neutral gas within the association. Carruthers, Heckathorn & Opal (1978) have detected NGC 206 as an extended source of far-ultraviolet radiation (at ≈ 1350 Å), and estimate that the flux is equivalent to that of ~ 240 B0 stars, in good agreement with the number of such stars found in the association.

4.4 H I AND CO EMISSION

Carbon monoxide has been detected at a number of points in the disc of M31 by Combes *et al.* (1977) but none in the nucleus (Rickard *et al.* 1977), in contrast with a number of nearby galaxies. Fig. 10 shows the positions (within the present survey area) observed by Combes *et al.* for CO emission on an integrated H I map. A detailed comparison between the distributions of H I and CO emission was not possible, because of the limited number of positions observed for CO emission. The correlation of CO detections with H I emission in Fig. 10 is not unexpected, since several of the points were chosen to coincide with dust features. However, it is significant that six out of seven detections, but only two out of six upper limits, occur where the H I intensity is $> 1000\,\mathrm{K\,km\,s^{-1}}$. No CO was detected at the point designated as M31-4SW in Table 5(b), where the integrated H I brightness is $2800\,\mathrm{K\,km\,s^{-1}}$. This is a surprising result, since M31-4SW is contiguous with four detections along arm *D* (Fig. 10), and all five points lie in a very dark dust lane coincident with the ridge of H I emission (Plate 3). These results are in agreement with a similar comparison made by Emerson (1978) using H I data of lower resolution.

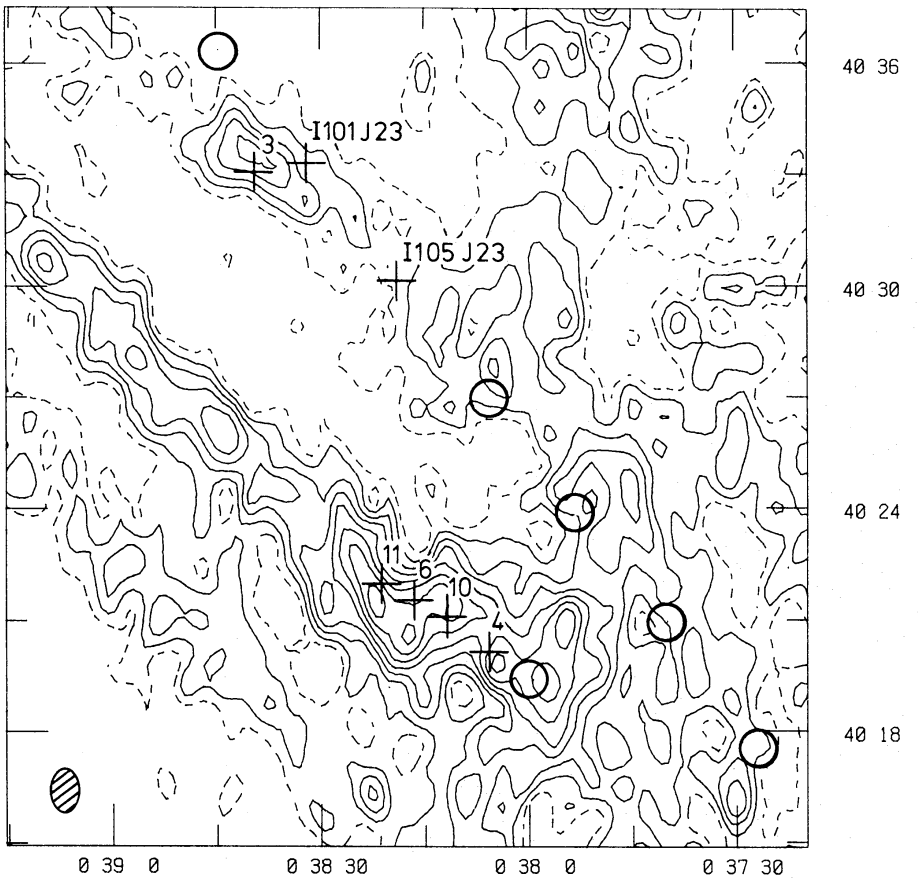

Figure 10. Integrated hydrogen map of the south-west region of M31, with superimposed positions of carbon monoxide observations from Combes *et al.* (1977). The contour interval is 400 K km s^{-1}, with the first contour shown dashed. Numbered crosses mark the positions of CO detections, and circles (with diameters equal to the HPBW of the CO observations) mark positions where no CO was found.

Table 5. Carbon monoxide observations of M31.

(a) Detection of CO emission

Observed point	Carbon monoxide			Integrated hydrogen		
	T_A	profile width	peak velocity	Intensity	profile width[1]	mean velocity[2]
	(K)	(km/s)	(km/s)	(K km/s)	(km/s)	(km/s)
I101 J23	0.30 ± 0.03	25 ± 5	-521 ± 3	1000 ± 130	30 ± 3	-529 ± 2
I105 J23	0.20	17	-510	550	25	-524
M31 - 3	0.15	15	-514	1600	23	-521
M31 - 4	0.13	25	-537	2350	32	-530
M31 - 6	0.31	16	-516	2700	37	-508
M31 - 10	0.10	15	-527	2850	32	-521
M31 - 11	0.15	20	-505	2800	35	-502

(b) Upper limits to CO emission (3σ = 0.09 K)

Observed point	Integrated hydrogen intensity (K km/s)
I97 J23	150 ± 30[3]
I109 J23	1000 ± 130
I113 J23	1100
I117 J23	750
I121 J23	850
M31 - 4SW[4]	2800

Notes : (1) Corrected for instrumental broadening.
(2) Derived from half-power points of profiles.
(3) From 1.9 × 2.9 arcmin resolution HI map.
(4) Point lies 1.2 arcmin SW of M31 - 4.

A detailed point-by-point comparison between the CO and H I observations is given in Table 5; since the beam sizes are very similar (1.0 × 1.0 and 0.8 × 1.2 arcmin respectively), the observations refer to similar linear scales. Table 5(a) shows that there is excellent agreement between the measured CO and H I velocities, with a mean difference $< 1\,\mathrm{km\,s^{-1}}$. The H I velocities were derived from the half-power points rather than the peaks of the profiles, but in all cases the differences due to asymmetric profiles were $< 2\,\mathrm{km\,s^{-1}}$. However, the three CO detections in the H I arm segment *B* (namely I101 J23, I105 J23 and M31–3) show numerically smaller radial velocities than those of H I emission (corresponding to slower rotation about the nucleus), whilst the opposite is found for the CO detections in arm *D*. These differences cannot be accounted for by the effect of velocity gradients across the H I and CO beams. Variations in CO profile widths from point to point are reflected in the H I profile widths: the mean ratio of CO width to H I width is 0.63 ± 0.15. Since both profiles are resolved in velocity, and the beam sizes are very similar, this is unlikely to be an instrumental effect. The lower dispersion in the CO profiles may imply that the thickness of the CO layer is less than that of H I. However, any comparison of the velocity data is complicated by the fact that the column density of CO is not simply related to its integrated brightness, but depends on the kinetic temperature. This has the effect of weighting the CO clouds in the beam unequally, and may explain some of the differences in the velocity profiles noted above. It is therefore not surprising that no correlation has been found between integrated H I brightness and integrated CO brightness for each position in Table 5(a).

4.5 NEUTRAL HYDROGEN AND THE COMPANION GALAXIES

The systemic velocity of M32 (= NGC 221) is $-190\,\mathrm{km\,s^{-1}}$ (de Vaucouleurs, de Vaucouleurs & Corwin 1976), at the extreme end of the velocity range covered by the present survey, so no H I emission associated with M32 could be observed. The H I emission found in the direction of M32 has radial velocities ~ -380 to $-370\,\mathrm{km\,s^{-1}}$, and is clearly associated with the disc of M31, rather than with M32.

No H I emission was detected by the present survey in NGC 205 (= M110) although the systemic velocity of $-239\,\mathrm{km\,s^{-1}}$ lay within the observed velocity range; the primary beam response at the position of NGC 205 was only 30 per cent. However, a survey with the Half-Mile telescope by Warner & Baldwin (private communication) has detected H I in NGC 205. The observational details (where different from those of the present survey) are given in Table 6, together with optical data on NGC 205 from de Vaucouleurs *et al.* (1976), and a description of the H I detection. The weak H I emission feature has a mass $\sim 3 \times 10^5 M_\odot$, and lies 1.5 arcmin south of the centre of NGC 205; the measured H I velocity differs by only $5\,\mathrm{km\,s^{-1}}$ from the systemic velocity.

NGC 205 is unusual for an elliptical galaxy in that it contains some bright blue Population I stars; Hodge (1973) has estimated that the mass of Population I stars lies between $\sim 5 \times 10^5$ and $5 \times 10^6 M_\odot$. Since dust clouds are also seen in the central parts of NGC 205, it is not surprising that H I gas has been found as well. The nearest dust cloud to the H I is 0.7 arcmin to the east (no. 4 in Hodge 1973), and may be associated with it. Most of the OB stars in NGC 205 are confined to a complex of diameter ~ 350 pc centred roughly on the nucleus; the H I feature is probably associated with this complex, and comprises at least 10 per cent of its mass.

Planetary nebulae may account for the observed neutral hydrogen in NGC 205; Ford & Jenner (1975) have estimated that the rate of hydrogen mass loss from planetary nebulae in M32 is $\sim 6 \times 10^{-4} M_\odot\,\mathrm{yr^{-1}}$, and this rate may be appropriate for NGC 205, since similar numbers have been detected in both companions (Ford & Jacoby 1978). The observed

Table 6. Detection of neutral hydrogen in NGC 205.

Map centre	RA	$0^h\ 37^m\ 36^s$
(1950.0)	dec	$41^o\ 25'\ 00''$
Mean epoch of survey		1975.5
Largest spacing		298.7 m
Number of spacings		48
Synthesized beamwidth		1.9 × 2.9 arcmin
Velocity coverage		-432 to -23 km/s
Position of NGC205 nucleus	RA	$0^h\ 37^m\ 38^s.4$
(1950.0)	dec	$41^o\ 24'\ 54''$
Position of HI detection	RA	$0^h\ 37^m\ 34^s$
(1950.0)	dec	$41^o\ 23'\ 24''$
Velocity of NGC205 nucleus (optical)		-239 km/s
Velocity of HI feature(1)		-234 ± 5 km/s
Dispersion of HI feature(2)		15 ± 5 km/s
Mass of HI feature		$(3 \pm 1) \times 10^5\ M_\odot$

Notes :

(1) Derived from half-power points of profile

(2) FWHP, corrected for instrumental broadening.

HI mass in NGC 205 could have been produced at this rate in $\sim 5 \times 10^8$ yr, in the absence of star formation. However, the gas consumption rate of the complex of OB stars (estimated from its mass and age given by Hodge 1973) is ~ 0.02–$0.1 M_\odot\,\mathrm{yr}^{-1}$, so it is unlikely that replenishment of the interstellar medium by planetary nebulae can support the present rate of star formation.

5 Spiral structure in M31

The spiral structure of M31 has been analysed by many authors using widely differing methods (Baade 1963; Arp 1964; Emerson 1974; Kalnajs 1975; Simien *et al.* 1978), but no general agreement has yet been reached regarding the overall pattern. Both the number of spiral arms and their sense of winding are in doubt, and these ambiguities are due to two main causes: (a) the pitch angle of any reasonable spiral (whether leading or trailing) must be small ($\lesssim 10°$), reflecting the fact that most spiral-arm tracers lie in near-circular arcs; (b) the unfavourable inclination of the disc requires the use of a large deprojection factor ~ 4.5 to produce a 'rectified' view of the spiral structure; any deprojected pattern of arm tracers is consequently very sensitive to the assumed orientation of the disc and to the presence of relatively small warps in it (Arp 1964).

A number of well-defined spiral arm segments are revealed by the high-resolution HI map of the present survey, and these are at least as useful as optical objects for tracing a large-scale spiral pattern. Section 5.1 discusses the relation of neutral hydrogen to the other principal tracers of spiral structure (dust, OB associations and HII regions), and Section 5.2

considers the evidence for a large-scale spiral pattern in the disc of M31. Unfortunately, the problems mentioned above prevent a definite conclusion from being reached, even with the addition of the data on neutral hydrogen.

5.1 SPIRAL ARMS IN H I AND OTHER POPULATION I MATERIAL

Fig. 2 shows a number of short H I arm segments taken from the 0.8×1.2 and 1.9×2.9 arcmin resolution maps (Figs 1 and 4), and it is clear that several of these should be joined to form longer portions of spiral arms. The identity of many of the arm segments is uncertain near the major axis, where they lie almost along the line-of-sight, and this section makes use of the correlations discussed in Section 4 to interpret the H I data. Continuity of the spiral pattern is the main argument used here, so that no arm segments may be joined which conflict with the optical picture, where this is unambiguous. An alternative method using Fourier series analysis (Kalnajs 1975) is not attempted here, as H I data at this resolution are as yet available for only one half of the galaxy.

Baade (1963) traced spiral arms using dust and OB stars, and numbered them N1–7 and S1–7 in order of their crossings of the major axis; this notation is adopted here for the optical spiral arms. N4 and S4 are the most clearly defined optical arms (Simien *et al.* 1978, Fig. 5b); arm *C* closely follows N4, whilst the dust lane on the inner edge of arm S4 lies along the H I arm segment *D*. The optical arms join near the bright OB association NGC 206, and so segments *C* and *D* are part of a larger H I arm. This then implies that the innermost H I arm segments *A* and *B* must form the H I counterpart of arm S3, and that the short segment *E* is probably a branch of arm *C–D*, as it apparently has a large pitch angle.

Arm S5 is traced optically by a string of OB associations (Fig. 7) and by H II regions (Plate 4), and the corresponding arm segments are *F* and *H*. (These are barely separated and may be part of the same arm.) The optical data suggest that arm *F* continues across the major axis into arm *G*, so that the outer limit of H I emission at high resolution is marked by the larger H I arm *H–F–G*; arm *I* may represent a branch of this arm. The outer arm *L* is traced by the OB associations OB180–185, and its continuation into arm *M* seems certain, even though only OB188 and Andromeda IV are visible in this area. Arm segments *J*, *K* and *N* are not well developed, and have no obvious relation to the other H I arms, although arm *N* may be a continuation of the outer arm *L–M*.

Simien *et al.* (1978) have found that a one-armed leading spiral pattern fits the observed distributions of H II regions and OB associations. The best-fitting spiral curve also fits a number of the H I arm segments from the present survey, although it joins them up in an unexpected way; arms *B* and *C* are part of a larger arm in this picture, as are *D*, *F* and *H*. Whilst it is possible that the joining of *B* and *C* may be correct, it is very unlikely that *D* joins on to *F*, since its turning point is well defined and coincides with that of Baade's arm S4. This lack of continuity suggests that a simple one-armed spiral represents an over-simplification of the true structure, which is almost certainly distorted.

5.2 LARGE-SCALE SPIRAL STRUCTURE

The following H I arm segments have been shown (Section 5.1) to consist of parts of larger arms: *A* and *B* are associated with Baade's arm S3; *C* and *D* with S4; *H*, *F* and *G* with S5; *L*, *M* and *N* with S6. Fig. 2 shows that no large-scale pattern can be seen in these longer arms, and that the sense of winding is not clear, even for individual arms. Any large-scale pattern must be considerably distorted, and this could be the result of two distinct effects.

First, the spiral pattern may not be adequately represented by a logarithmic spiral over the whole disc, possibly because of interaction with the companion galaxy M32. Secondly, the disc may be warped in a way which distorts the spiral pattern as seen from a direction highly inclined to the rotation axis.

Arp (1964) found that a simple model of a warp could explain the distribution of H II regions in terms of a two-armed trailing (logarithmic) spiral. The turning points (positions of maximum distance from the minor axis) of the H I arms *A–B* and *C–D* are displaced to the south-east side of the major axis. This distortion is also seen in the corresponding optical arms (S3 and S4); photometry of the disc by Richter & Högner (1963) gives a clear impression that the position angle should be decreased from 38 to $\approx 34^\circ$ in the region of these two arms.

Byrd (1978) has modelled the gravitational effect of M32 on the spiral structure in the disc of M31. Two features of this model agree well with the H I observations discussed in this paper. First, it provides an explanation for the poor separation of arms *F* and *H*, since the model disc is severely warped in this area; double-peaked velocity profiles are found here, because arms at different radii have been warped so that they appear along the same line-of-sight. Secondly, it explains the peculiar morphology of the H I arm *L* (Fig. 4), which leaves the main 'ring' of emission at a large apparent pitch angle. In the model of Byrd (1978) the corresponding arm is S6, which has a very similar appearance.

The warp models of Arp (1964) and Byrd (1978) have shown that considerable distortions of the disc of M31, and hence also the spiral structure, are present. Until the geometry of any warping is known accurately, attempts to fit a spiral pattern (whether leading or trailing) are unlikely to be persuasive. It must therefore be concluded that the spiral arm tracers available at present do not allow a large-scale spiral pattern to be distinguished in M31.

6 Conclusions

This paper has presented observations of neutral hydrogen in the south-west of M31 at a resolution of 0.8 × 1.2 arcmin. The main conclusions are summarized as follows:

(i) Much of the neutral hydrogen forms long narrow arm-like segments, which are resolved by the telescope beam and are separated by several times their widths, except near the minor axis.

(ii) An optical depth of $\tau = 0.22$ has been found in the direction of the continuum source 5C 3.107, implying that the H I spin temperature is ~ 220 K. Except in a few areas where brightness temperatures exceed ~ 60 K, self-absorption is not significant.

(iii) Dust and H I gas are well mixed on scales ~ 100 pc, and both lie on the inner edges of bright optical arms.

(iv) The relative distributions of H I and OB associations differ on the two sides of the major axis, confirming the importance of obscuration in the visual appearance of a disc system seen nearly edge-on.

(v) There is a strong correlation between the surface densities of H II regions and H I gas on a scale comparable with the beam size. The number of H II regions detected in areas of highest H I density is limited by obscuration.

(vi) Segments of spiral arms can be seen in the H I distribution up to ~ 25 kpc from the nucleus, and the arms traced in H I complement those which are distinguished optically. The spiral structure of M31 remains ambiguous on account of the large disc inclination and the probable existence of significant warping in it.

Acknowledgments

Thanks are due to many members of the Radio Astronomy Group for assistance with these observations, in particular to Mrs S. E. G. Hales for help with the data reduction. I am grateful to Mr P. J. Warner, Dr K. Newton and Dr J. E. Baldwin for many helpful discussions, and to Dr J. R. Shakeshaft for constructive comments on the manuscript. Financial support from the SRC is gratefully acknowledged.

References

Allen, R. J. & Goss, W. M., 1979. *Astr. Astrophys. Suppl.*, **36**, 135.
Arp, H., 1964. *Astrophys. J.*, **139**, 1045.
Baade, W., 1963. *Evolution of Stars and Galaxies*, p. 73, ed. Payne-Gaposchkin, C., Harvard University Press, Cambridge, Massachusetts.
Baade, W. & Arp, H., 1964. *Astrophys. J.*, **139**, 1027.
Bajaja, E. & Gergely, T. E., 1977. *Astr. Astrophys.*, **61**, 229.
Berkhuijsen, E. M., 1977. *Astr. Astrophys.*, **57**, 9.
Byrd, G. G., 1978. *Astrophys. J.*, **226**, 70.
Carruthers, G. R., Heckathorn, H. M. & Opal, C. B., 1978. *Astrophys. J.*, **225**, 346.
Combes, F., Encrenaz, P. J., Lucas, R. & Weliachew, L., 1977. *Astr. Astrophys.*, **61**, L7.
de Vaucouleurs, G., de Vaucouleurs, A. & Corwin, H. G., Jr., 1976. *Second Reference Catalogue of Bright Galaxies*, University of Texas, Austin.
Emerson, D. T., 1974. *Mon. Not. R. astr. Soc.*, **169**, 607.
Emerson, D. T., 1976. *Mon. Not. R. astr. Soc.*, **176**, 321.
Emerson, D. T., 1978. *Astr. Astrophys.*, **63**, L29.
Ford, H. C. & Jacoby, G. H., 1978. *Astrophys. J.*, **219**, 437.
Ford, H. C. & Jenner, D. C., 1975. *Astrophys. J.*, **202**, 365.
Gillespie, A. R., 1974. *PhD thesis*, University of Cambridge.
Hartwick, F. D. A., 1971. *Astrophys. J.*, **163**, 431.
Henderson, A. P., 1979. *Astr. Astrophys.*, **75**, 311.
Hodge, P. W., 1973. *Astrophys. J.*, **182**, 671.
Kalnajs, A. J., 1975. *La Dynamique des Galaxies Spirales*, p. 103, ed. Weliachew, L., Editions du CNRS, Paris.
Marscher, A. P. & Brown, R. L., 1978. *Astrophys. J.*, **220**, 474.
Newton, K. & Emerson, D. T., 1977. *Mon. Not. R. astr. Soc.*, **181**, 573.
Newton, K., 1978. *PhD thesis*, University of Cambridge.
Pellet, A., Astier, N., Viale, A., Courtès, G., Maucherat, A., Monnet, G. & Simien, F., 1978. *Astr. Astrophys. Suppl.*, **31**, 439.
Pooley, G. G., 1969. *Mon. Not. R. astr. Soc.*, **144**, 101.
Richter, N. & Högner, W., 1963. *Astr. Nachr.*, **287**, 261.
Rickard, L. J., Palmer, P., Morris, M., Turner, B. E. & Zuckerman, B., 1977. *Astrophys. J.*, **213**, 673.
Roberts, M. S., 1966. *Astrophys. J.*, **155**, 639.
Roberts, W. W., 1969. *Astrophys. J.*, **158**, 123.
Rots, A. H. & Shane, W. W., 1975. *Astr. Astrophys.*, **45**, 25.
Shane, W. W., 1975a. *La Dynamique des Galaxies Spirales*, p. 257, ed. Weliachew, L., Editions du CNRS, Paris.
Shane, W. W., 1975b. *La Dynamique des Galaxies Spirales*, p. 217, ed. Weliachew, L., Editions du CNRS, Paris.
Simien, F., Athanassoula, E., Pellet, A., Monnet, G., Maucherat, A. & Courtès, G., 1978. *Astr. Astrophys.*, **67**, 73.
Spenser, J. H. & Burke, B. F., 1975. *Astrophys. J.*, **199**, 611.
van den Bergh, S., 1964. *Astrophys. J. Suppl.*, **9**, 65.
van den Bergh, S., 1966. *Astr. J.*, **71**, 219.
van den Bergh, S., 1972. *Astrophys. J.*, **171**, L31.
van der Kruit, P. C., 1972. *Astrophys. Lett.*, **11**, 173.
van der Kruit, P. C. & Katgert, P., 1972. *Astrophys. Lett.*, **11**, 181.
Winter, A. J. B., 1975. *PhD thesis*, University of Cambridge.